International Journal of Heat and Mass Transfer 52 (2009) 5827–5840

Contents lists available at ScienceDirect

International Journal of Heat and Mass Transfer

journal homepage: www.elsevier.com/locate/ijhmt

Numerical model and effectiveness correlations for a run-around heat recovery system with combined counter and cross flow exchangers

Alireza Vali, Carey J. Simonson *, Robert W. Besant, Gazi Mahmood

Department of Mechanical Engineering, University of Saskatchewan, 57 Campus Drive, Saskatoon, SK, Canada S7N 5A9

ARTICLE INFO

Article history:
Received 30 January 2009
Received in revised form 31 July 2009
Accepted 31 July 2009
Available online 24 September 2009

Keywords:
Counter/cross flow
Effectiveness
NTU
Heat capacity ratio
Run-around heat exchanger

ABSTRACT

A two-dimensional steady-state numerical model is developed to study the heat transfer in a run-around heat recovery system with two exchangers each with a combination of counter and cross (counter/cross) flow between parallel plates or membranes. A finite difference method is used to solve the steady-state equations of continuity, momentum and heat transfer. The simulated values for the effectiveness of each counter/cross flow heat exchanger and the overall run-around system are used to develop effectiveness correlations which agree within ±2% of the simulated effectiveness of individual heat exchangers and overall system. It is shown that the effectiveness of this new run-around heat exchanger (RAHE) falls between the effectiveness of similar run-around systems with either two cross-flow exchangers or two counter-flow exchangers. For a given total surface area of the exchangers, the highest overall sensible effectiveness is achieved with exchangers which have a small exchanger aspect ratio and relatively small solution flow inlet and outlet lengths.

1. Introduction

Without energy recovery, ventilation air increases energy consumption of buildings since outdoor air must be cooled or heated to bring it close to the indoor thermal comfort conditions. About 20–40% of the overall energy consumption of HVAC system is consumed for ventilation air-conditioning in most commercial buildings. In buildings that require 100% outdoor air to meet ventilation standards (e.g. hospitals), this fraction can be even higher (e.g. 50–60%) [1].

Air-to-air energy recovery systems can be employed in buildings to precondition the supply air by using the exhaust air energy to reduce the HVAC energy consumption. This also reduces the size of heating and cooling facilities when the indoor air quality is satisfactory [2]. The air-to-air energy recovery system investigated in this paper is a run-around heat exchanger (RAHE), shown in Fig. 1, which is composed of two separate heat exchangers and a coupling liquid which can be antifreeze aqueous ethylene glycol solution. The solution is pumped in a closed loop between the heat exchangers. The pumped liquid gains heat from the air stream in one exchanger and releases the heat to air stream in the other one. Unlike other air-to-air heat or energy recovery devices, the run-around system does not require the supply and exhaust air ducts to be located side by side. This gives run-around systems an advantage over other available systems when cross contamination is a concern (e.g. surgery rooms in hospitals and chemical and biological laboratories) or in retrofit applications where the exhaust and supply air ducts have already been installed far apart.

One of the first studies on the run-around system was published by London and Kays [3]. It was found that at a constant *NTU*, the system had its optimum performance when the heat capacity rates of the air and coupling liquid were equal [3]. Few studies have been done on the RAHE systems in recent years. Forsyth and Besant [4,5] developed a numerical simulation to investigate the performance and design of a RAHE with two coil heat exchangers. They also proposed that the total life cycle costs should be taken into account for the system rather than effectiveness at one operating condition to obtain the optimum design. The model developed by Forsyth and Besant did not agree well with the experimental data because the heat transfer correlations used did not include all the complex factors that existed in the experimental system.

Bennett et al. [6,7] included wavy fins and the effects of the thermal contact resistance between the fins and coils in the numerical model developed by Forsyth and Besant [4,5]. The computations of Bennett et al. [6,7] agreed with the experimental results from an installed system. Dhital et al. [8] studied the maximum outdoor air ventilation rate and the energy performance of office buildings with and without the run-around heat recovery systems to investigate the energy saving of the RAHE system. They showed that using a RAHE system in a building could save significant amount of energy and allow the ventilation airflow rate to be increased without increasing the energy consumption. Fan et al. [9,10] developed a numerical model to investigate the heat and

* Corresponding author. Tel.: +1 306 966 5479; fax: +1 306 966 5427.
E-mail address: carey.simonson@usask.ca (C.J. Simonson).

0017-9310/$ - see front matter © 2009 Elsevier Ltd. All rights reserved.
doi:10.1016/j.ijheatmasstransfer.2009.07.020

Nomenclature

C	heat capacity rate (W/K)
c_p	specific heat capacity [J/(kg K)]
Cr	heat capacity ratio
D_h	hydroulic diameter (mm)
d	channel dimension (mm)
$HVAC$	Heating, ventilating and air-conditioning
h	convective heat transfer coefficient [W/(m^2 K)]
k	thermal conductivity [W/(m K)]
$\dot{m}$	mass flow rate (kg/s)
NTU	number of transfer units
P	Pump
Pe	Peclet number
q	heat transfer rate (W)
$RAHE$	run-around heat exchanger
Re	Reynolds number
T	temperature (K)
t	temperature (^{o}C)
U	overall heat transfer coefficient [W/(m^2 K)]
u, v	velocity components (m/s)
x, y, z	Coordinates
x_0, y_0, z_0	heat exchanger dimensions (mm)
x_i	header dimension (mm)

Greek symbols

ψ	stream function
δ	thickness of the plate (mm)
ρ	density (kg/m^3)
ε	effectiveness
ε_o	overall effectiveness of run-around heat recovery system
λ	convergence criterion
∂, ∇	differential operators

Subscripts

A	air
$Counter$	Counter-flow heat exchanger
$Counter/cross$	heat exchanger with a combination of cross and counter-flow
$Cross$	Cross flow heat exchanger
E	exhaust
f	fluid
in	inlet
L	liquid
max	maximum
min	minimum
o	overall RAHE system
out	outlet
S	supply

coupled heat and moisture transfer in the run-around systems using two flat-plate cross flow exchangers.

It is well known that the counter-flow exchangers have significantly higher effectiveness compared to the cross flow exchanger effectiveness. Therefore, it is desirable to have an exchanger in the RAHE with airstreams and coupling fluid flowing in the counter-flow arrangement in the exchanger. However, a pure counter-flow exchanger with simple headers located adjacent to each other is difficult to construct in the limited space available in most HVAC ducting systems. The design in this paper incorporates counter-flow heat exchanger with cross flow inlet and outlet headers, i.e. counter/cross flow (Fig. 2). This counter/cross flow design allows the air and coupling fluid to enter and leave the exchanger at right angles relative to each other and simplifies the header design and installation of the exchangers.

Correlations using the dimensionless geometric, flow, and thermal parameters for predicting the performance of heat exchangers are presented in [11–13]. Counter or cross flow exchanger correlations are presented in these references, but there is no correlation available for the counter/cross flow heat exchangers. The present study is aimed to develop the effectiveness correlations from a numerical model of a counter/cross flow exchanger. New effectiveness correlations are developed to predict the overall sensible effectiveness of the run-around heat recovery system using two counter/cross flow exchangers. The effects of dimensionless geometric, flow, and thermal parameters on the exchanger and overall system effectivenesses are predicted. These new effectiveness correlations can help manufacturers and HVAC engineers to design and develop low cost high energy efficient heat recovery systems.

2. Numerical model

The numerical model investigates the performance of a run-around heat exchanger (RAHE), shown in Fig. 1, with two identical flat-plate counter/cross flow heat exchangers, shown in Fig. 2,

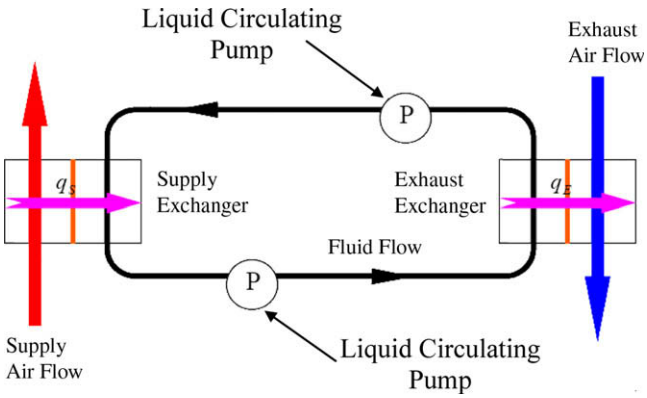

Fig. 1. Schematic diagram of a run-around heat exchanger (RAHE).

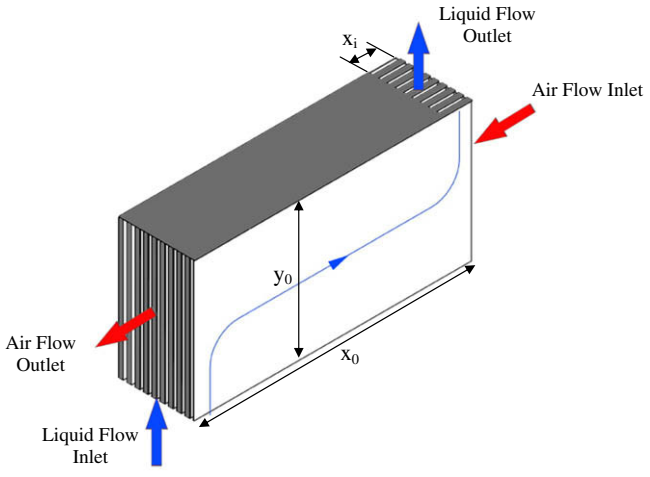

Fig. 2. Schematic of a flat-plate counter/cross flow heat exchanger.

under the steady-state operating conditions. In the exchanger presented in Fig. 2, liquid enters from bottom header (inlet header) at the left hand corner of the exchanger and leaves the exchanger from the top header at the right hand corner, after traveling a S-shaped path line through the exchanger liquid channels. Both the top and bottom headers have a length of x_i (Figs. 2 and 3), which is less than the exchanger length (x_0). To avoid having a large pressure drop in the air stream, the air flows uniformly in a straight path from right to left in Fig. 2 through each exchanger air channel.

The exchanger consists of several individual and identical modules. A schematic of a module with the coordinate system for the mathematical model and the air and the liquid flow paths are shown in Fig. 3. The module contains one air channel adjacent to one liquid channel. Fig. 3 also shows wall thickness between the air and liquid channels, and channel dimensions. One complete exchanger consists of 10 such modules presented in Fig. 3. As the effects of module geometry on exchanger effectiveness are investigated using dimensionless groups, definite values of (x_0, y_0, x_i) are not presented.

2.1. Assumptions

The following assumptions are used in the development of the numerical model:

1. No heat transfer occurs between the surroundings and the heat exchangers or the coupling fluid flow as the outer walls of the exchangers and liquid flow lines are adequately insulated.
2. For each liquid–air channel pair, heat is transferred only normal to the plate (z-direction in Fig. 3) as the temperature gradient across the exchanger ($T_{out} - T_{in} < 10$ °C) and plate thickness (Fig. 3) are typically small.
3. Steady-state conditions.
4. The air and liquid solution have uniform properties at the inlets of each heat exchanger.
5. Axial conduction in each fluid is negligible since $Pe > 20$ in the channels [14]
6. Both the air and liquid flows are laminar as $Re < 2000$ in both the air and liquid sides.
7. Heat transfer is estimated based on the bulk mean velocities and temperatures in the model. That is, T_A and T_L do not vary along z-direction (Fig. 3) and fluid temperatures are only changing in x and y-directions (i.e. $T_A(x, y)$ and $T_L(x, y)$).
8. The channel gaps, d_L and d_A, are small (Fig. 3), so the entrance lengths for the fluid flow and heat transfer are very small with respect to the exchanger length, x_0. Typical entrance lengths are 2 and 3 mm for flow and temperature, respectively, for an exchanger of 1 m long. Based on the channel geometry Graetz number is large [13] and the effects of momentum and thermal entrance lengths are neglected in the model.
9. Liquid and air flow distributions are independent from heat transfer as the air and liquid flows are dominated by the pressure difference between the inlet and outlet pressure and the typical temperature differences that exist in HVAC systems are small (i.e. $T_{out} - T_{in} < 10$ °C). Using this assumption, the momentum equation can be decoupled from the heat transfer equation.
10. Temperature and velocity distributions are similar in all pairs of liquid–air channels in each exchanger due to the uniform module geometry, fluid flows, and boundary conditions. That is, the effects of mal-distribution of inlet or internal flows are not included in the model.
11. Condensation and frosting are neglected.
12. Supply and exhaust heat exchangers are identical.

2.2. Governing equations

According to the Hele-Shaw experiments, the steady flow of viscous fluid at low Reynolds number between two closely spaced parallel plates can be considered as a plane two-dimensional ideal flow for the distribution of bulk mean streamlines [15]. In this study, the liquid flows slowly through the liquid channels ($Re < 10$) and the channel size, d_L, is very small with respect to the exchanger length, x_0 (e.g. $d_L/x_0 = 0.003$). For steady flow, the second-order Laplace equation for the stream function (ψ) can be applied to determine the bulk mean liquid velocity:

$$\nabla^2\psi = 0 \tag{1}$$

The bulk mean velocity components are:

$$u = \frac{\partial\psi}{\partial y}; \quad v = -\frac{\partial\psi}{\partial x} \tag{2}$$

The air temperature, T_A, in a module is determined by balancing the heat transfer through the plate with the change in the energy content of the air as it flows through the exchanger:

$$-\frac{2Uy_0}{C_A}(T_A - T_L) = \frac{\partial T_A}{\partial x} \tag{3}$$

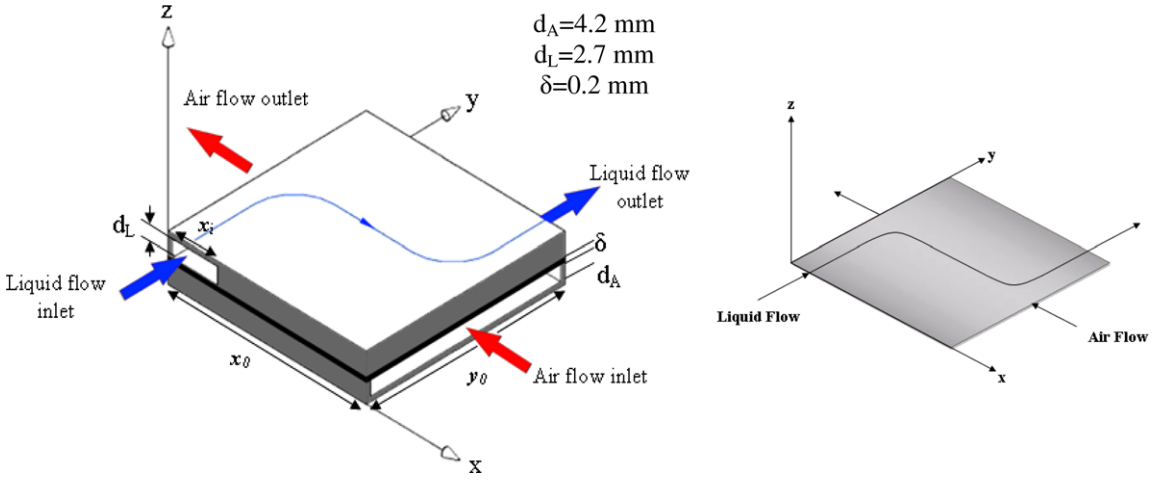

Fig. 3. A module of a counter/cross flow heat exchanger made of an air channel and a liquid channel with coordinate system.

Table 1
Thermo physical properties of air and aqueous ethylene glycol solution.

Property	Correlation or value
$c_{p,L}$	$3588.554 + 2.8441 \times t - 1.135 \times 10^{-4} \times t^2$ J/(kg K) $(-10\ ^\circ\text{C} \leqslant t \leqslant 70\ ^\circ\text{C})$
ρ_L	$1051.7797 - 0.2776 \times t - 2.4339 \times 10^{-3} \times t^2$ kg/m^3 $(-10\ ^\circ\text{C} \leqslant t \leqslant 70\ ^\circ\text{C})$
k_L	$0.42906 + 1.3396 \times 10^{-3} \times t - 5.9288 \times 10^{-6} \times t^2$ W/(m K) $(-10\ ^\circ\text{C} \leqslant t \leqslant 70\ ^\circ\text{C})$
$c_{p,A}$	1010 J/(kg K)
ρ_A	1.17 kg/m^3
k_A	0.0263 W/(m K)

In the liquid stream, the heat transfer rate through the plate surface is balanced by the change in the liquid temperature, T_L, at any point (x, y) as the liquid flows in exchanger liquid channels:

$$2U(T_A - T_L) = \rho_L c_{p,L} d_L \left(u\frac{\partial T_L}{\partial x} + v\frac{\partial T_L}{\partial y} \right) \tag{4}$$

Note that the conservation of mass dictates air velocity to have only x-component. The overall heat transfer coefficient, U, between the air flow and liquid flow is,

$$U = \left[\frac{1}{h_L} + \frac{\delta}{k} + \frac{1}{h_A} \right]^{-1} \tag{5}$$

For fully developed laminar flow between parallel plates with the constant heat flux boundary conditions, the convective heat transfer coefficient is given by the following equation [13].

$$\frac{hD_h}{k_f} = 8.24 \tag{6}$$

where D_h is the hydraulic diameter (i.e. $D_h = 2d_A$ or $2d_L$). It is known that for counter-flow heat exchanger the constant heat flux boundary condition is valid due to its temperature variation through the exchanger [13]. This assumption can be applied here as the counter/cross flow heat exchanger is close to the counter-flow heat exchanger. Eqs. (1)–(4) are applicable for both the supply and exhaust heat exchangers. The correlations [1] and values [13] applied for the thermo-physical properties of air and liquid are listed in Table 1 where the liquid is aqueous ethylene glycol with 30% concentration, and the relative humidity and temperature of the air are 50% and 35 °C, respectively.

2.3. Boundary conditions

The boundary conditions for solving the flow and temperature distributions within each heat exchanger are summarized in Fig. 4. Also, note that the boundary conditions in Fig. 4 are valid for both the supply and exhaust heat exchangers. In a RAHE, without heat loss/gain in the liquid connecting pipes, the bulk mean temperature of the coupling liquid at the outlet of one exchanger is the same as the inlet liquid temperature for the other exchanger downstream. Therefore, as shown in Fig. 5:

$$T_{L,in,S} = T_{L,out,E} \tag{7}$$

$$T_{L,in,E} = T_{L,out,S} \tag{8}$$

The air inlet conditions must be specified to simulate the RAHE system. The specific values of air inlet conditions are provided when the results are discussed later. However, the effectiveness of each heat exchanger and the RAHE system will not be affected by the inlet condition unless the temperature differences across the exchanger are very large and cause large variation of the air and liquid properties.

2.4. Solution scheme

The governing equations and boundary conditions are discretized using an implicit finite difference method. The backward differencing scheme is used for solving temperature distribution on both the air and liquid sides. For liquid flow distribution, a central differencing discretization scheme is used. The computational domain of each air and liquid channel in a module is divided into 200×200 spatial grids of uniform size along x–y. Sensitivity studies show that the effect of higher number of nodes on the predicted overall effectiveness of the RAHE system is trivial. For example, overall effectiveness changes less than 0.1% for 300×300 grids compared to 200×200 grids. The discretized equations are solved using a Gauss-Seidel iteration technique.

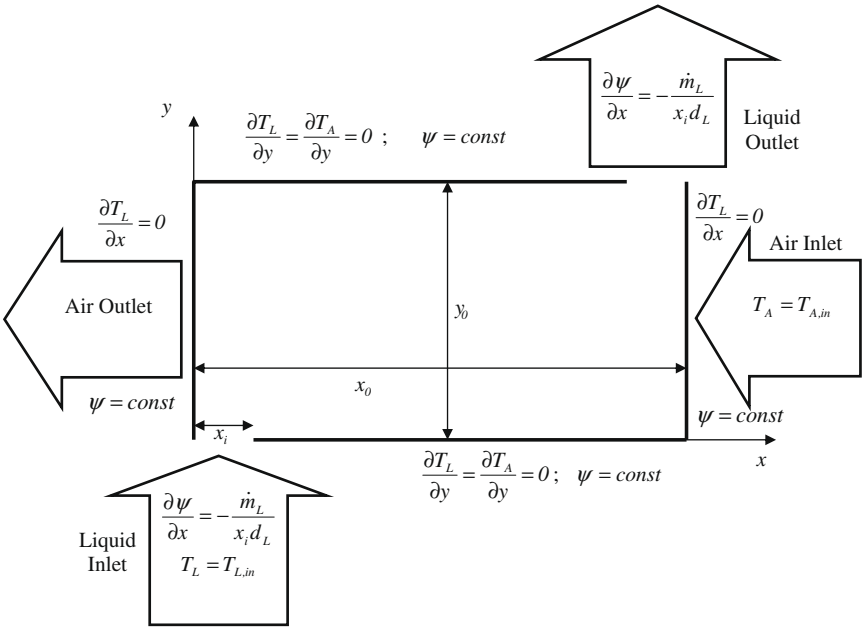

Fig. 4. The boundary conditions for solving Eqs. (1)–(4).

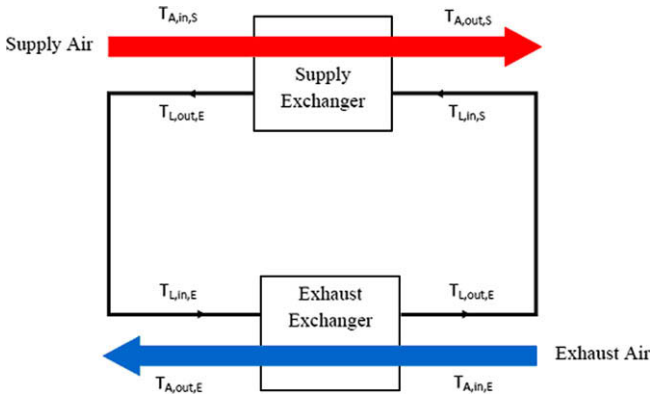

Fig. 5. Schematic diagram showing the inlet and outlet condition of each exchanger of the run-around heat recovery system.

First, the numerical model is setup to solve for the liquid velocity components of the bulk mean liquid flow (Eqs. (1) and (2)). The bulk mean liquid flow distribution determined from solving Eq. (1) is shown in Fig. 6 based on the assumptions listed above and the boundary conditions provided in Fig. 4. Then, the velocity components are used in the exchanger heat transfer equations to obtain the temperature and heat flux in the fluids (Eqs. (3) and (4)). By coupling the two heat exchangers in a closed loop (Eqs. (7) and (8)), the model simulates the RAHE system.

The outlet mean temperatures of the heat exchangers need to be computed to determine the heat transfer in the exchangers and inlet liquid temperature at the downstream heat exchanger according to Eqs. (7) and (8). The liquid and air temperatures are not constant across the outlet widths. The following equations are used to calculate the outlet bulk mean temperatures of the air and liquid leaving the supply or exhaust heat exchanger.

$$T_{A,out} = \frac{1}{\dot{m}_A c_{p,A} y_0} \int_{y_0} \dot{m}_A c_{p,A} T_A dy \tag{9}$$

$$T_{L,out} = \frac{1}{\dot{m}_L c_{p,L} x_i} \int_{x_i} \dot{m}_L c_{p,L} T_L dx \tag{10}$$

Subscript S or E can be applied on the left hand side of Eq. (9) or (10) based on the heat exchanger being solved for.

When the energy transfer between the system and the surrounding is negligible, the energy transfers in the supply and exhaust exchangers must be balanced at steady-state. As a result, the RAHE reaches steady-state when

$$q_S = q_E \tag{11}$$

where q_S and q_E are the energy transfer between the liquid and air in the supply and the exhaust exchangers, respectively:

$$q_S = C_{A,S}(T_{A,in,S} - T_{A,out,S}) = C_{L,S}(T_{L,out,S} - T_{L,in,S}) \tag{12}$$

$$q_E = C_{A,E}(T_{A,in,E} - T_{A,out,E}) = C_{L,E}(T_{L,out,E} - T_{L,in,E}) \tag{13}$$

The following equation can be used as the steady-state criterion for computational iterations to converge.

$$\frac{|q_S - q_E|}{(q_S + q_E)/2} \le \lambda \tag{14}$$

The value of 1×10^{-5} is used for λ. The sensitivity of the results to a smaller λ value is very marginal. For example, if $\lambda = 1 \times 10^{-6}$ is used, the effectiveness changes less than 0.1% compared to that obtained with $\lambda = 1 \times 10^{-5}$.

3. Dimensionless groups

The following dimensionless groups are used to develop the effectiveness correlations for the RAHE and illustrate the effects of different design parameters on the effectiveness: (i) $NTU = \frac{2Ux_0y_0}{C_{min}}$, (ii) $Cr = \frac{C_{min}}{C_{max}}$, (iii) $\frac{y_0}{x_0}$ = the aspect ratio of the heat exchanger (Fig. 4), (iv) $\frac{x_i}{x_0}$ = entrance length ratio (Fig. 4). In the above relations, C_{min} is the minimum of (C_A, C_L) and C_{max} is the maximum of (C_A, C_L) in each heat exchanger.

Based on the definition of effectiveness [11,13], effectiveness of the individual heat exchanger is:

$$\varepsilon = \frac{C_A(T_{A,in} - T_{A,out})}{C_{\min}(T_{A,in} - T_{L,in})} \tag{15}$$

where C_{min} is defined above. In the equation above, subscript S or E can be incorporated to denote the effectiveness of supply or exhaust heat exchanger, respectively.

The overall sensible effectiveness of the RAHE can be defined as:

$$\varepsilon_o = \frac{C_{A,S}(T_{A,in,S} - T_{A,out,S})}{C_{\min}(T_{A,in,S} - T_{A,in,E})} = \frac{C_{A,E}(T_{A,out,E} - T_{A,in,E})}{C_{\min}(T_{A,in,S} - T_{A,in,E})} \tag{16}$$

where C_{min} is the minimum of $C_{A,S}$ and $C_{A,E}$ and inlet and outlet temperatures are shown in Fig. 5.

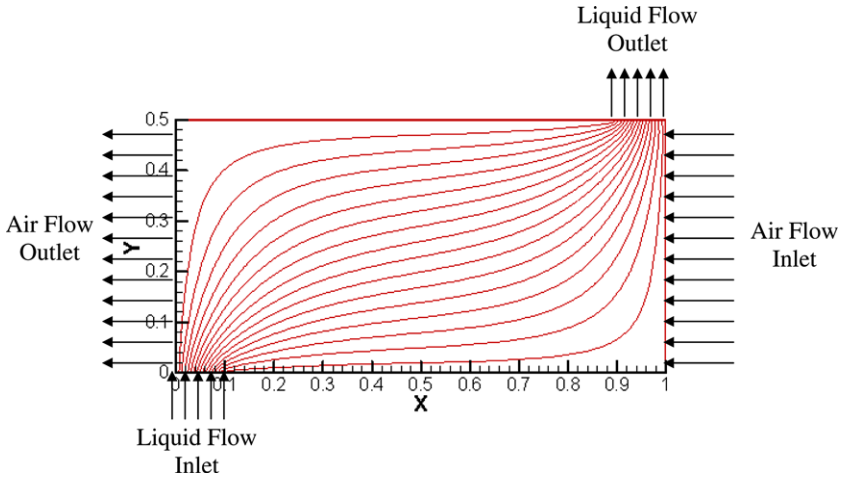

Fig. 6. Bulk mean liquid flow distribution in counter/cross flow heat exchanger.

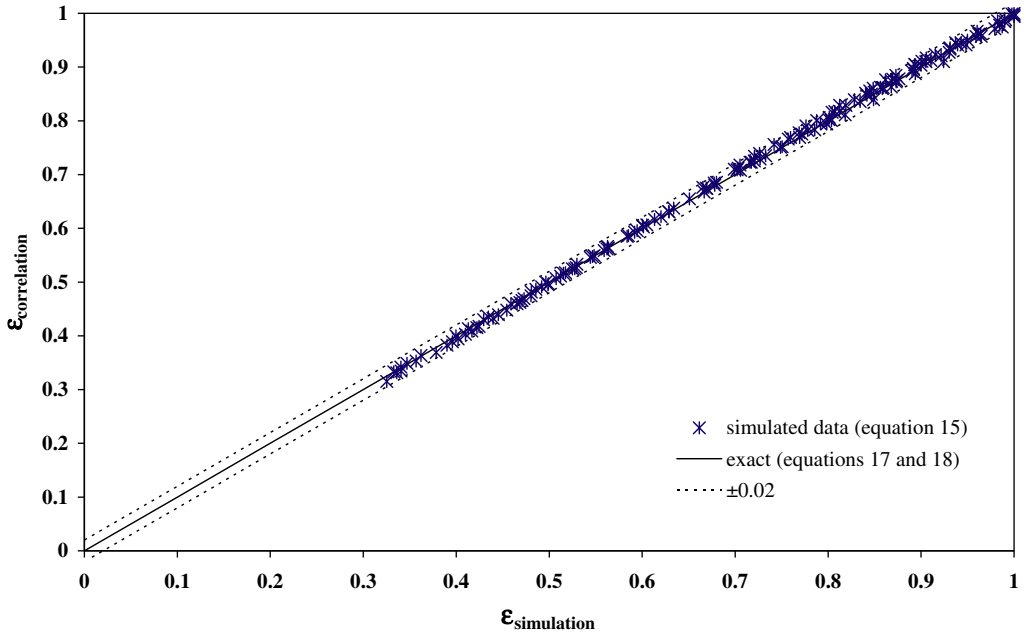

Fig. 7. Effectiveness of the flat-plate cross flow heat exchanger and counter-flow heat exchanger from correlations (17) and (18) compared to the simulated effectiveness using Eq. (15) for $0 < Cr \leqslant 1$ and $0 < NTU \leqslant 15$.

4. Verification of the model

The model presented in this paper can be used to predict effectiveness of the cross, counter or counter/cross flow heat exchangers. The effectiveness of cross flow heat exchangers with both fluids unmixed can be calculated from following correlation [13]:

$$\varepsilon_{cross} = 1 - exp\left[\left(\frac{1}{Cr}\right)(NTU)^{0.22}\{exp[-Cr(NTU)^{0.78}] - 1\}\right] \tag{17}$$

For counter-flow heat exchangers, the effectiveness can be determined with the following analytical solution [13]:

$$\varepsilon_{counter} = \frac{1 - exp(-NTU(1 - Cr))}{1 - Crexp(-NTU(1 - Cr))} \tag{18}$$

In the above two equations, *NTU* and *Cr* are the same as defined in the previous section. The correlations presented in Eqs. (17) and (18) are widely accepted in practice to predict the effectiveness of the cross and counter-flow heat exchangers.

Fig. 7 shows the effectiveness values for the cross flow heat exchanger and the counter-flow heat exchanger calculated by the numerical model, Eq. (15), for over 160 simulated cases that are compared with the effectiveness values from Eqs. (17) and (18). In Fig. 7, when the simulation and the effectiveness correlations predict exactly the same values the data points must lie on the

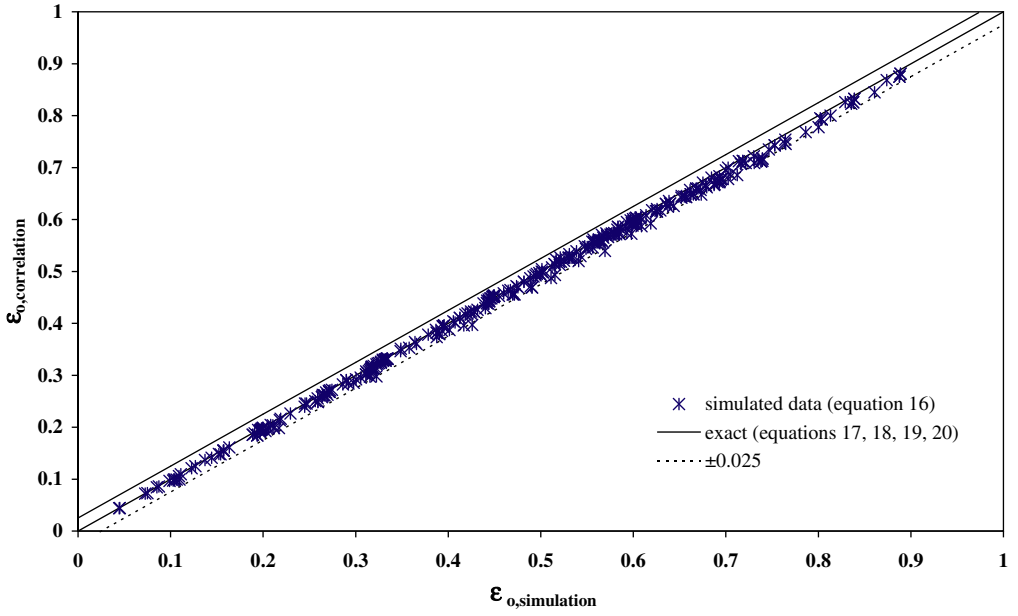

Fig. 8. Overall effectiveness of RAHE made of two identical flat-plate cross flow heat exchangers or counter-flow heat exchangers from Eqs. (17)–(20) compared with the simulated effectiveness, Eq. (16), for $0 < Cr \leqslant 1$ and $0 < NTU \leqslant 15$.

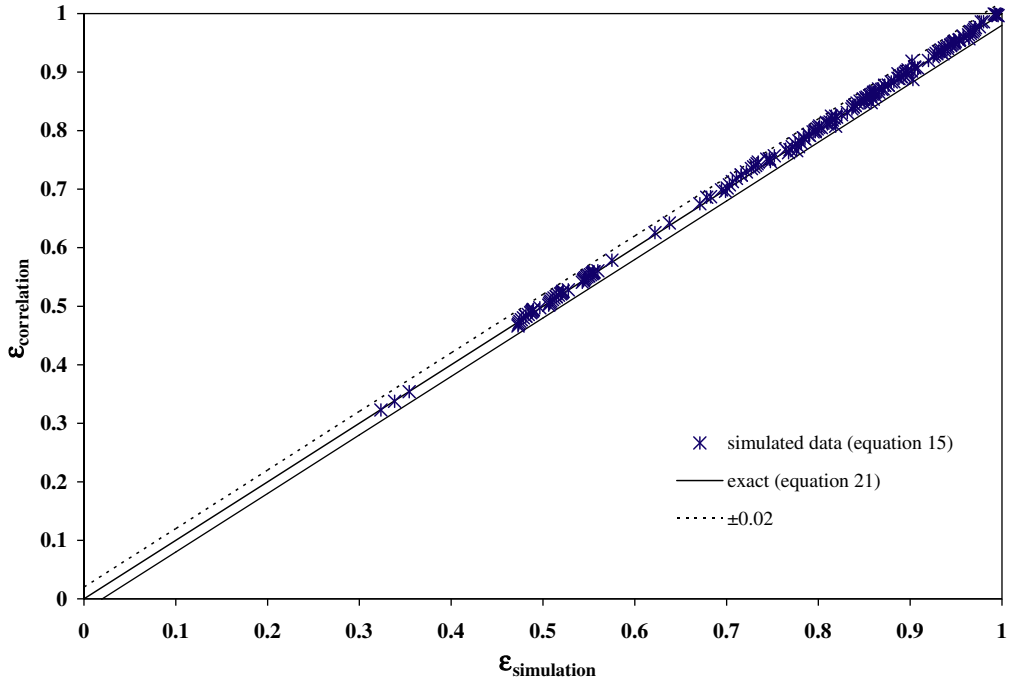

Fig. 9. Effectiveness of the counter/cross flow heat exchanger from Eq. (21) compared to the simulated effectiveness using Eq. (15) for $0 < Cr \leqslant 1$, $0 < NTU \leqslant 15$, $0 < x_i/x_0 \leqslant 0.25$ and $0 < y_0/x_0 \leqslant 1$.

solid line which is referred as exact. The dash lines show the region where the discrepancy between the simulation and the effectiveness correlations is within ±0.02. As shown in Fig. 7, the simulated effectivenesses of cross flow heat exchanger and counter-flow heat exchanger predicted by the numerical model (Eq. (15)) for over 160 simulated data points agree with the effectivenesses calculated by Eqs. (17) and (18) within ±0.02 for $0 < Cr \leqslant 1$ and $0 < NTU \leqslant 15$.

Zeng et al. [16] developed a correlation for the RAHE system with two identical heat exchangers and the same air mass flow rates in supply and exhaust heat exchangers ($\dot{m}_{A,S} = \dot{m}_{A,E}$), which is the focus of this paper. The effectiveness of the RAHE system is calculated from following equations:

$$\frac{1}{\varepsilon_o} = \frac{1}{\varepsilon_E} + \frac{1}{\varepsilon_S} - Cr, \quad \text{for} \quad C_A \leq C_L \tag{19}$$

$$\frac{1}{\varepsilon_o} = \frac{1}{Cr}\left(\frac{1}{\varepsilon_E} + \frac{1}{\varepsilon_S} - 1\right), \quad \text{for} \quad C_A > C_L \tag{20}$$

The key parameters here are ε_S and ε_E that can be computed from the effectiveness correlations presented previously (Eqs. (17) and (18)). A comparison between the effectiveness data obtained from

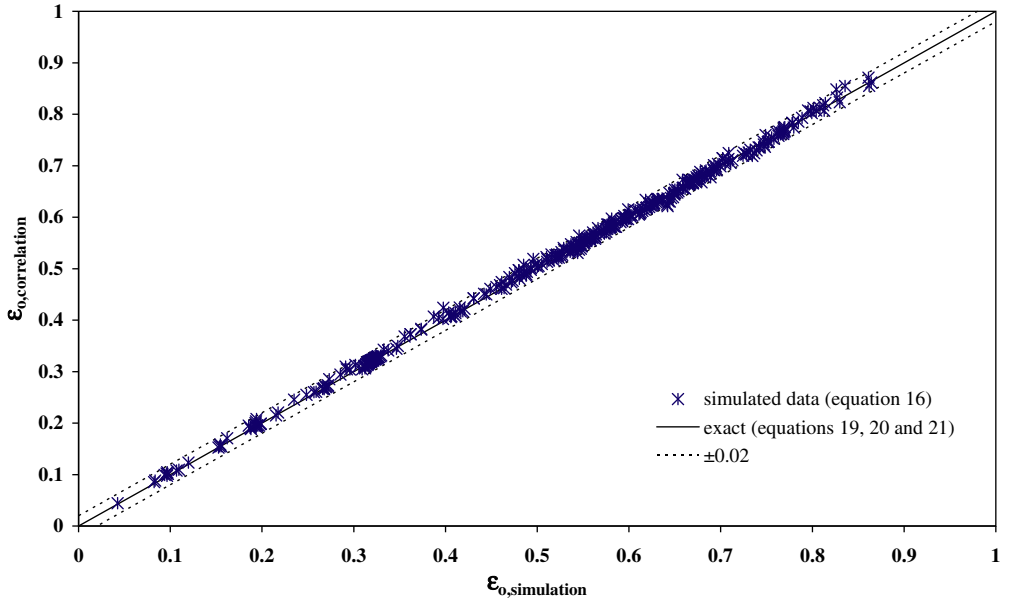

Fig. 10. Overall effectiveness of a RAHE with two identical counter/cross flow heat exchangers correlated by Eqs. (19)–(21) is compared with the simulated effectiveness (Eq. (16)) for $0 < C_L/C_A \leqslant 10$, $0 < Cr \leqslant 1$, $0 < NTU \leqslant 15$, $0 < x_i/x_0 \leqslant 0.25$, and $0 < y_0/x_0 \leqslant 1$.

Eqs. (19) and (20) and the results from the numerical model using Eq. (16) is shown in Fig. 8. The effectivenesses of the run-around heat recovery system with two identical cross flow or two counter-flow heat exchangers calculated from the correlations agree with the simulated effectivenesses within ±0.025 for $0 < Cr \leqslant 1$ and $0 < NTU \leqslant 15$ for over 350 simulated data points.

5. Effectiveness correlations

The simulated data can be correlated into functional relationships for convenient engineering design. Sensitivity studies on the effectiveness of the counter/cross flow heat exchanger with respect to different design parameters reveal that the effectiveness depends on *NTU*, *Cr*, aspect ratio (y_0/x_0), and entrance ratio (x_i/x_0).

The effects of the entrance ratio (x_i/x_0) on the effectiveness of the counter/cross flow heat exchanger are minor for the range of $0 < x_i/x_0 \leqslant 0.25$. For example, with $NTU = 3$, $Cr = 10$ and $y_0/x_0 = 0.25$, the effectiveness of the heat exchanger changes by less than 0.02 as (x_i/x_0) changes from 0 to 0.25. Due to practical considerations, an entrance ratio of greater than 0.25 is unlikely. The smaller entrance ratio means, the predominantly counter-flow heat exchanger (see Fig. 12). x_i/x_0 can be neglected in the effectiveness correlation when the entrance ratio is less than 0.25.

Fig. 6 clearly indicates that the liquid streamlines are combinations of the counter (*x*-axis) and cross (*y*-axis) direction liquid flow. It is therefore expected, for the same total heat transfer surface area, the effectiveness of a counter/cross flow heat exchanger ($\varepsilon_{counter/cross}$) will fall between the effectiveness of a pure counter-flow exchanger ($\varepsilon_{counter}$) and a pure cross flow exchanger (ε_{cross}). Therefore, the effectiveness correlation for a counter/cross flow heat exchanger ($\varepsilon_{counter/cross}$) is proposed to have the following form:

$$\varepsilon_{counter/cross} = \left[\left(\frac{y_0}{x_0}\right)\left(1+\frac{NTU}{200}\right)\varepsilon_{cross} + \left(1-\frac{y_0}{x_0}\right)\varepsilon_{counter}\right], \quad \text{for} \quad 0 < x_i/x_0 \leq 0.25 \tag{21}$$

In the above correlation, $\varepsilon_{counter}$ and ε_{cross} can be obtained from Eqs. (17) and (18) with the same *NTU* and *Cr* as those for simulated $\varepsilon_{counter/cross}$. This correlation can be used for the parameters $0 < y_0/x_0 \leqslant 1$ and $0 < x_i/x_0 \leqslant 0.25$.

In Fig. 9, the effectiveness of the counter/cross flow heat exchanger calculated from Eq. (21) is compared to the effectiveness calculated by the simulation from Eq. (15) for $0 < Cr \leqslant 1$, $0 < NTU \leqslant 15$, $0 < x_i/x_0 \leqslant 0.25$ and $0 < y_0/x_0 \leqslant 1$. Over 200 data points are presented from simulations. The data in Fig. 9 show that Eq. (21) agrees with the numerical model within ±0.02.

The correlations (Eqs. (19) and (20)) deduced from Zeng et al. [16] can be applied to validate numerical results for a RAHE system with two identical counter/cross flow heat exchangers. Eq. (21) is used to determine ε_S and ε_E for the counter/cross flow heat exchangers in the correlations. A comparison between the simulation using Eq. (16) and the data from Eqs. (19)–(21) for the RAHE is presented in Fig. 10. The input parameters for all the data in Fig. 10 include $0 < C_L/C_A \leqslant 10$, $0 < Cr \leqslant 1$, $0 < NTU \leqslant 15$, $0 < x_i/x_0 \leqslant 0.25$ and $0 < y_0/x_0 \leqslant 1$. As shown, the effectivenesses from the correlations for the RAHE with counter/cross flow heat exchangers agree with 400 simulated data points within ±0.02.

6. Applications and limitations of the correlation

The new correlation (Eq. (21)) is applied to show the effects of different design parameters on the effectiveness and the limitations which the correlation may have in predicting the effectiveness. These limitations are indicated relative to the results from simulations. The selected operating conditions of $T_{A,in}$=308.15 K (35 °C) and $T_{L,in}$=297.15 K (24 °C) are applied in the numerical model for a single heat exchanger.

As mentioned previously, a parameter in determining $\varepsilon_{counter/cross}$ is the entrance ratio (x_i/x_0) of the exchanger. The simulated effectiveness of the heat exchanger decreases with increasing (x_i/x_0) as shown in Fig. 11. On the other hand, the correlation (Eq. (21)) does not account for changes in the entrance ratio and predicts a constant effectiveness value of 0.72. The data in Fig. 11 are

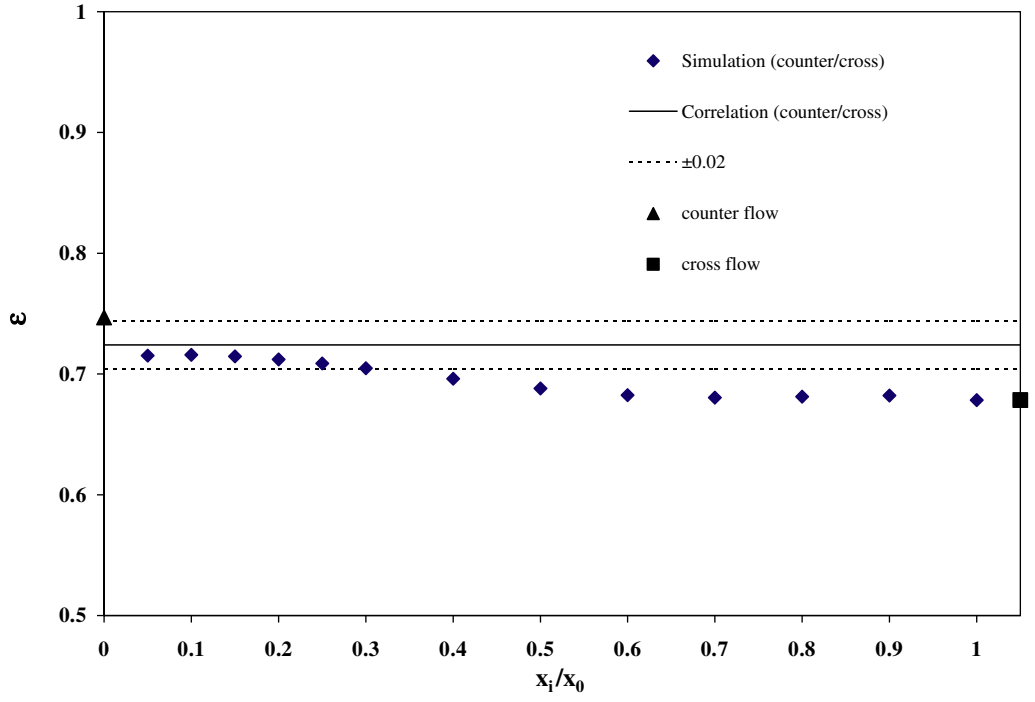

Fig. 11. Variation of the effectiveness of a counter/cross heat exchanger with entrance ratio, x_i/x_0, for $NTU = 3$, $Cr = 1$ and $y_0/x_0 = 0.25$. The simulated effectivenesses of pure cross flow and pure counter-flow exchangers are included for comparison.

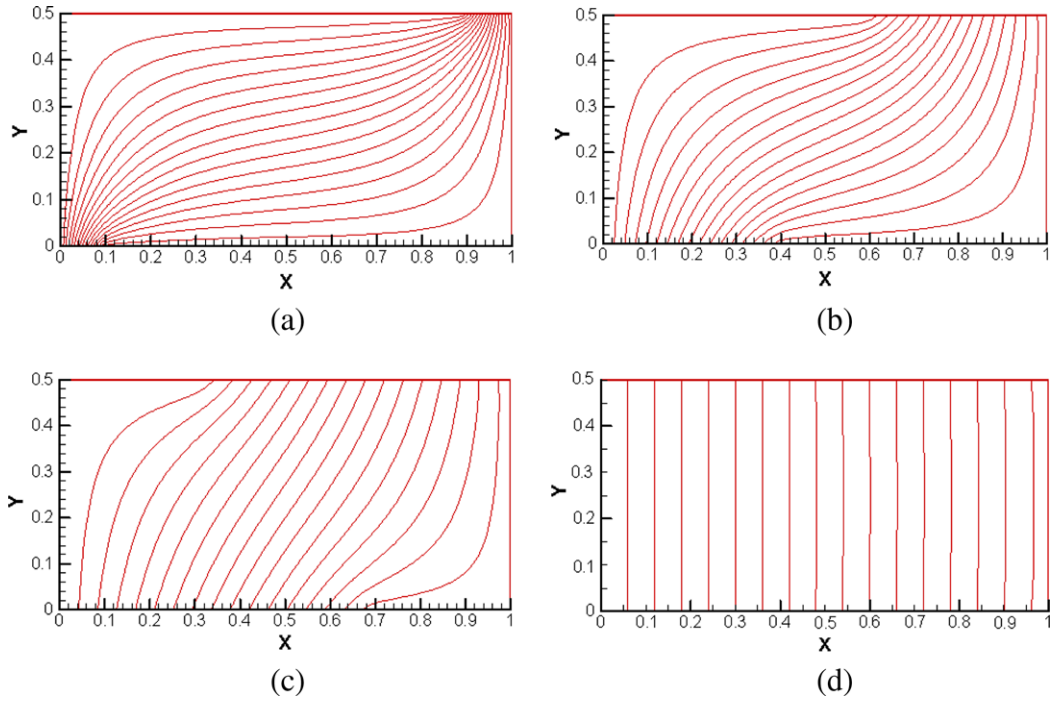

Fig. 12. Liquid stream lines in a counter/cross flow heat exchanger with the entrance ratio (x_i/x_0) of (a) 0.1, (b) 0.4, (c) 0.7 and (d) 1 when $y_0/x_0 = 0.5$.

presented for the same *NTU*, *Cr*, and y_0/x_0. It is unlikely to design a counter/cross flow heat exchanger with $x_i/x_0 > 0.25$ as $\varepsilon_{counter/cross}$ will be less than 0.7 according to Fig. 11, which is more than 4% smaller than the computed $\varepsilon_{counter}$ value of 0.75. As the effects of the entrance ratio on the effectiveness are trivial for $0 < x_i/x_0 \leqslant 0.25$ (less than ±0.02), this parameter was neglected in developing the correlation. Therefore, the correlation is limited to $0 < x_i/x_0 \leqslant 0.25$ and extrapolation of the correlation beyond an entrance ratio of 0.25 will lead to errors greater than 0.02 (Fig. 11). Also note that with $x_i/x_0 < 0.25$, the effectiveness of a counter/cross exchanger is always between the effectiveness of a pure counter-flow and a pure cross flow exchanger with the same *NTU* and *Cr*.

Fig. 12 shows the simulated streamline patterns in a counter/cross flow heat exchanger as the entrance ratio changes at a constant exchanger aspect ratio. As shown in Fig. 12, as the entrance ratio increases from $x_i/x_0 = 0.1$ to 1, the liquid flow patterns change from predominately counter-flow direction in Fig. 12(a) to predominately cross flow direction in Fig. 12(d). The horizontal liquid streamlines indicate a counter-flow arrangement as they are parallel and opposite to the air flow from right to left in

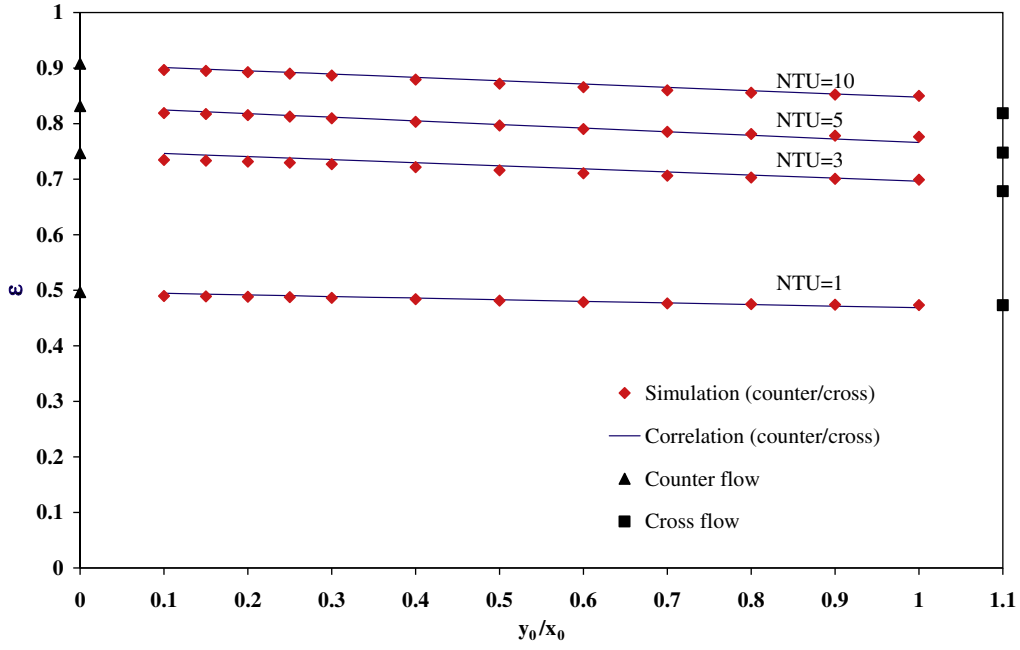

Fig. 13. Effectiveness of the counter/cross flow heat exchanger as a function of the aspect ratio (y_0/x_0) and *NTU* for *Cr* = 1 and $x_i/x_0 = 0.1$. The simulated effectivenesses of pure cross and pure counter-flow exchangers are included for comparison.

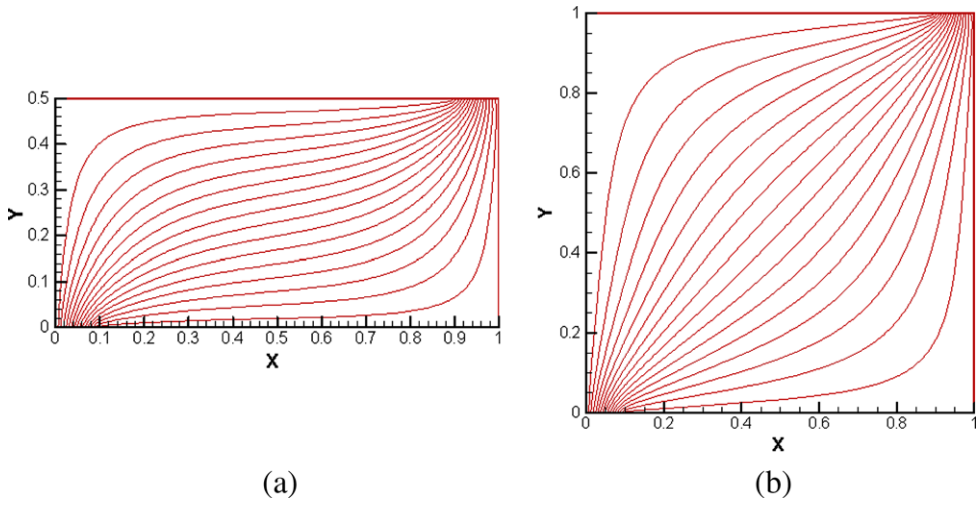

Fig. 14. Liquid stream lines in a counter/cross flow heat exchanger with the aspect ratio (y_0/x_0) of (a) 0.5 and (b) 1 when $x_i/x_0 = 0.1$.

Fig. 12. Exchanger effectiveness is higher for the counter-flow than it is for the cross flow (Fig. 11). This explains why simulated data in Fig. 11 decrease as x_i/x_0 increases. When x_i/x_0=1, the length of the inlet and outlet headers is equal to the exchanger length, which makes it a cross flow heat exchanger (Fig. 12(d)). The simulated effectiveness of counter/cross flow heat exchanger with x_i/x_0=1 in Fig. 11 equals the cross flow effectiveness with the same *NTU* and *Cr*.

The effects of the aspect ratio (y_0/x_0) and *NTU* on the effectiveness of counter/cross flow heat exchanger ($\varepsilon_{counter/cross}$) are shown in Fig. 13 for the case of $Cr = 1$ and $x_i/x_0 = 0.1$. For comparison, the effectivenesses of a pure cross flow heat exchanger and a pure counter-flow heat exchanger with the same *NTU* and *Cr* are also shown in Fig. 13. The simulated data from Eq. (15) are compared with data computed from Eq. (21) in Fig. 13. It can be seen that for a given *NTU*, $\varepsilon_{counter/cross}$ decreases from a value near $\varepsilon_{counter}$ to a value near ε_{cross} as the aspect ratio (y_0/x_0) increases from 0.1 to 1. It should be noted that *NTU* and *Cr* are the only dimensionless groups affecting the effectiveness of the cross flow or counter-flow heat exchanger. For a given y_0/x_0, effectiveness increases with *NTU* in Fig. 13 as the heat transfer rate increases at higher *NTU*. The correlation in Fig. 13 agrees well with the simulation (Eq. (15)).

The liquid flow distribution will change when the aspect ratio changes, which affects the exchanger effectiveness. Simulated liquid flow distributions for two designs with different aspect ratios are illustrated in Fig. 14. As the aspect ratio of the exchanger decreases from 1 to 0.5, liquid flows predominately in the counter-flow direction relative to the air (Fig. 14). Consequently, the effectiveness increases as y_0/x_0 decreases in Fig. 13. The predominant cross flow arrangement of the liquid flow at higher y_0/x_0 causes the effectiveness to decrease as y_0/x_0 increases.

In Fig. 15, computed $\varepsilon_{counter/cross}$ using Eqs. (15) and (21) is presented as a function of *NTU* and *Cr* when $y_0/x_0 = 0.5$ and $x_i/x_0 = 0.1$.

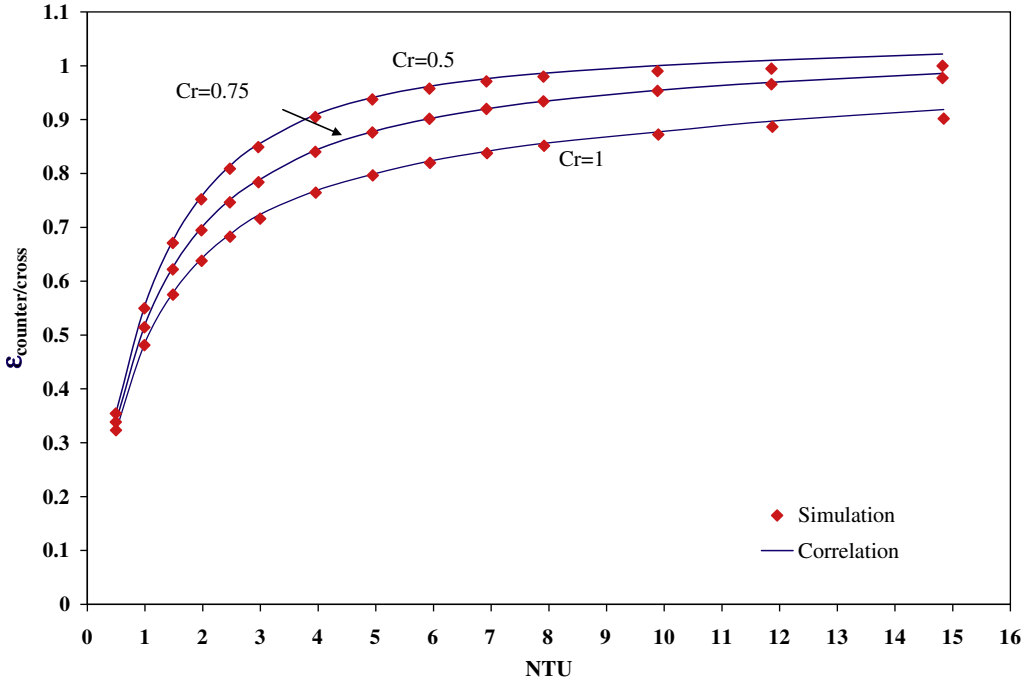

Fig. 15. Variation of the effectiveness of a counter/cross flow heat exchanger with *NTU* and *Cr*, $y_0/x_0 = 0.5$ and $x_i/x_0 = 0.1$.

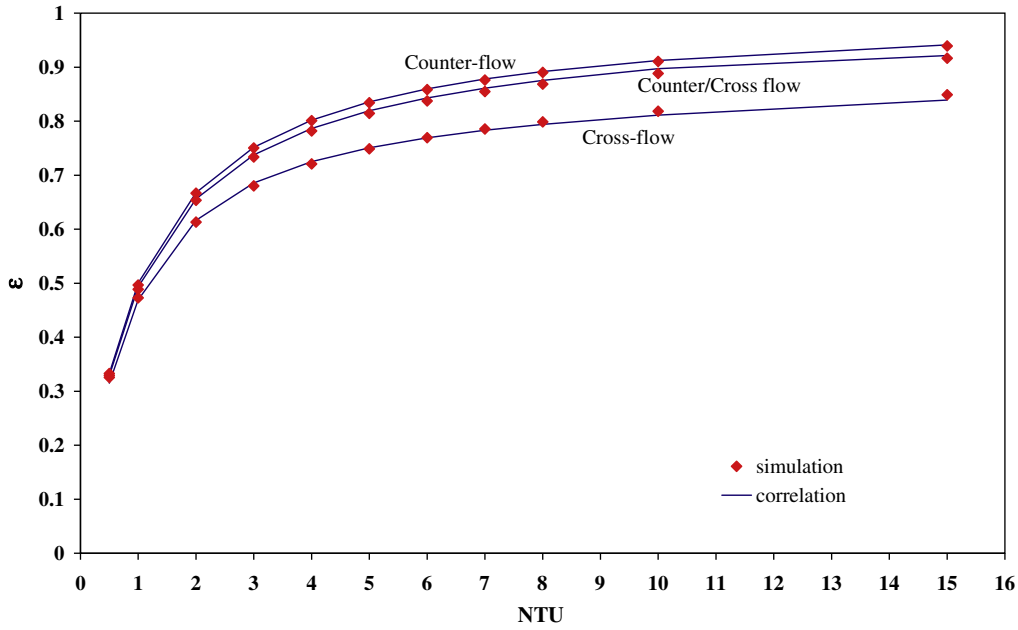

Fig. 16. Effectiveness of a single heat exchanger with pure cross flow, pure counter-flow and counter/cross flow arrangements as a function of *NTU* when $Cr = 1$. The counter/cross flow exchanger has $x_i/x_0 = 0.1$ and $y_0/x_0 = 0.25$.

Both the simulation (Eq. (15)) and correlation data (Eq. (21)) show that the effectiveness increases as *NTU* increases at constant *Cr*. Effectiveness in Fig. 15 also increases as *Cr* decreases at constant *NTU*. The close agreements between the simulation and correlation in Fig. 15 verify the correlation for a wide range of *NTU* and a range of $0.5 \leqslant Cr \leqslant 1$.

A direct comparison of effectiveness for three different heat exchangers: cross flow, counter-flow and counter/cross flow, is shown in Fig. 16 as *NTU* is varied when *Cr*=1. The effectiveness of the counter-flow exchanger is the highest, which is expected. The effectiveness of the counter/cross flow heat exchanger ($\varepsilon_{counter/cross}$) falls between the effectiveness of the counter-flow exchanger and cross flow exchanger for both the simulation and correlation. In this specific case where the aspect ratio and the entrance ratio of counter/cross flow exchanger are 0.25 and 0.1, respectively, $\varepsilon_{counter/cross}$ is close to $\varepsilon_{counter}$. The effectiveness of the counter/cross flow heat exchanger at *NTU* = 15 and *Cr* = 1 is improved by 8% compared to the effectiveness of the cross flow exchanger in Fig. 16.

The simulated overall effectiveness results using Eq. (16) for the RAHE with two identical counter/cross flow heat exchangers are

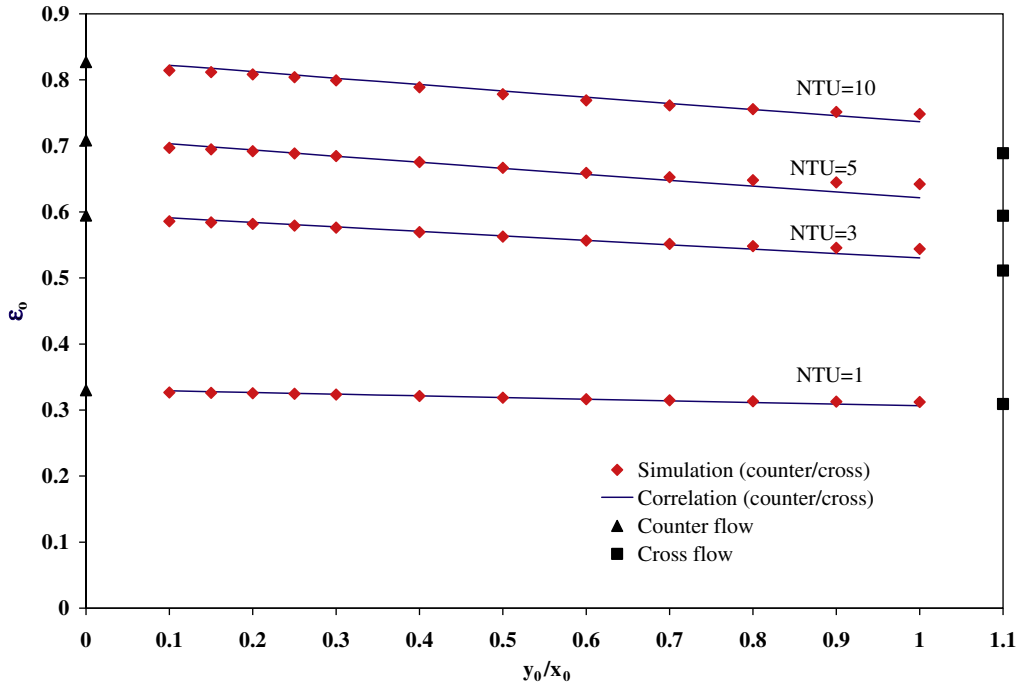

Fig. 17. Variations of the overall effectiveness of the RAHE system with two identical counter/cross heat exchangers with the aspect ratio and *NTU* when $Cr = 1$ and $x_i/x_0 = 0.1$ The simulated effectivenesses of pure cross flow and pure counter-flow exchangers are included for comparison.

compared with the correlations using Eqs. (19)–(21) in Figs. 17–19. The operating conditions for run-around system are $T_{A,in,S}$ = 308.15 K (35 °C) and $T_{A,in,E}$=297.15 (24 °C) in the simulations.

The effects of the aspect ratio (y_0/x_0) of the exchangers on the overall effectiveness of the RAHE ($\varepsilon_{o,counter/cross}$) are shown in Fig. 17 as *NTU* changes. As the aspect ratio decreases, $\varepsilon_{o,counter/cross}$ increases at a constant *NTU*. As shown in Fig. 17, $\varepsilon_{o,counter/cross}$ is close to $\varepsilon_{o,counter}$ when aspect ratio is small ($y_0/x_0 \approx 0$). The overall effectiveness at a constant aspect ratio, y_0/x_0, increases with *NTU* as heat transfer rate is higher for higher *NTU*. The *NTU* at a constant *Cr* in Fig. 17 is changed as both air and liquid flow rates changes. The correlations (Eqs. (19)–(21)) in Fig. 17 compare well with the simulated data using Eq. (16).

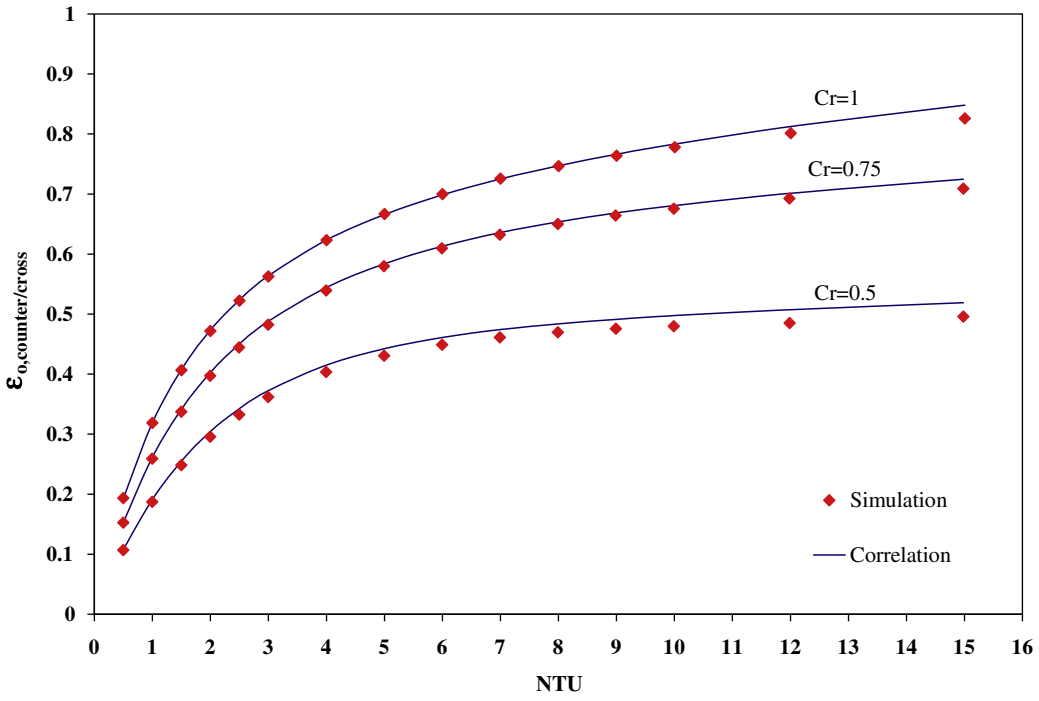

(a)

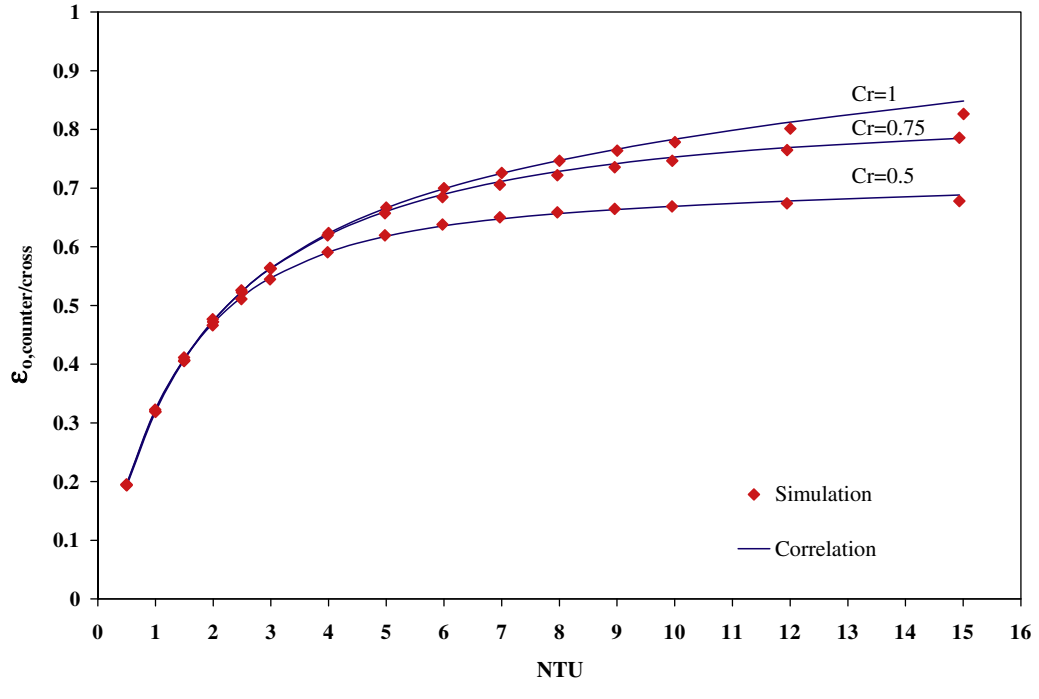

(b)

Fig. 18. Variation of overall effectiveness of RAHE system with two identical counter/cross flow heat exchangers with *NTU* and *Cr* for (a) $C_A > C_L$ and (b) $C_A < C_L$, x_i/x_0 = 0.1and y_0/x_0 = 0.5.

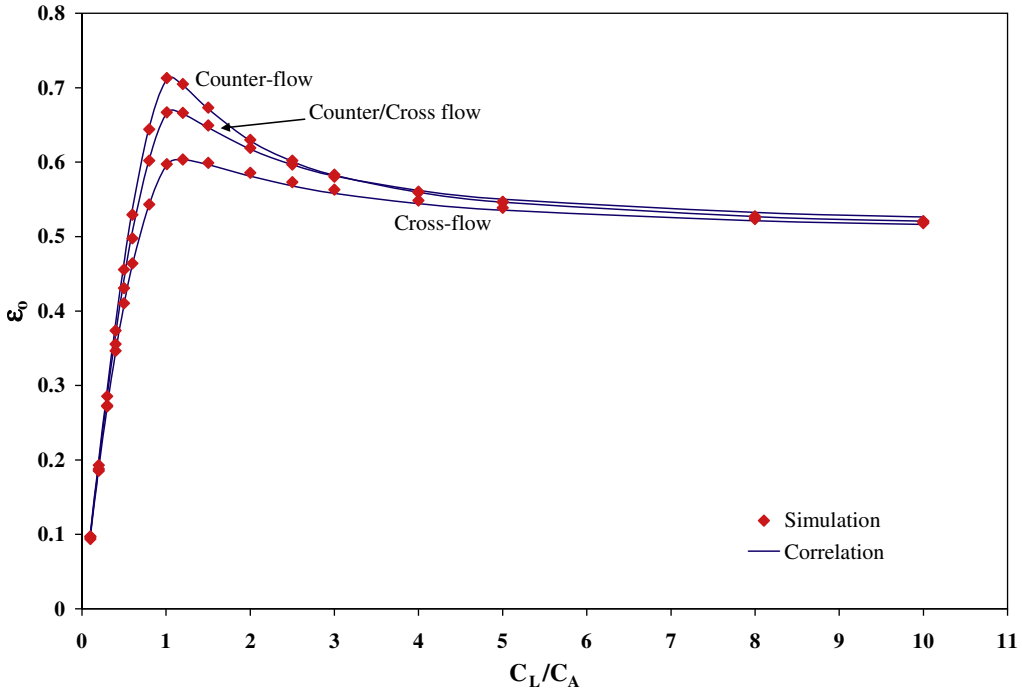

Fig. 19. Overall effectiveness of RAHE system with two identical counter-flow, counter/cross flow, and cross flow heat exchangers as a function of C_L/C_A when $NTU = 5$, $x_i/x_0 = 0.1$, and $y_0/x_0 = 0.5$.

Fig. 18 shows the effects of *NTU* and *Cr* on the overall effectiveness of the RAHE system. From Fig. 18, the overall effectiveness increases as *NTU* and *Cr* increase. The effectiveness of the system depends strongly on *Cr* for $NTU > 3$ in both Fig. 18(a) and (b). For $NTU < 3$, the effectiveness changes substantially with *NTU* at any value of *Cr*. Although the effectiveness of a single heat exchanger is the lowest when $Cr = 1$, the maximum effectiveness of RAHE occurs when $Cr = 1$ which shows that a heat exchanger must be treated differently when it is coupled with another exchanger in a run-around system. Similar trend of changing the overall effectiveness of RAHE with respect to *Cr* is observed by [3,9]. From a comparison between Fig. 18(a) and (b), it can be found that when $C_A > C_L$ the overall effectiveness is more sensitive to *Cr*. However, for $Cr < 1$ and $NTU > 3$, the overall effectiveness is higher when $C_A < C_L$ than when $C_A > C_L$.

When $NTU = 5$, $y_0/x_0 = 0.5$ and $x_i/x_0 = 0.1$, the overall effectivenesses of the RAHE system with two identical counter-flow, counter/cross flow, and cross flow heat exchangers are shown in Fig. 19 as a function of C_L/C_A. As expected, $\varepsilon_{o,counter}$ is the highest. $\varepsilon_{o,counter/cross}$ falls between $\varepsilon_{o,counter}$ and $\varepsilon_{o,cross}$. Also in Fig. 19, the maximum overall effectiveness occurs when $C_L = C_A$ for all types of heat exchangers. The counter/cross flow design improves the maximum overall effectiveness of the RAHE system at $C_L/C_A = 1$ by 7% compared to that of the RAHE system with two cross flow heat exchangers. The difference in ε_o between different heat exchanger systems tends to diminish at $C_L/C_A > 6$. The good agreement between the simulation and correlation for the RAHE system with counter/cross flow exchangers verifies the accuracy of the correlation for a wide range *NTU* and C_L/C_A values.

Although it is not presented, it is found that $\varepsilon_{o,counter/cross}$ changes by about 0.02 over the range of $0 < x_i/x_0 \leqslant 0.25$ for $NTU = 15$. For lower *NTU* values, $\varepsilon_{o,counter/cross}$ is less sensitive to the entrance ratio.

7. Summary and conclusions

A numerical model of a run-around heat recovery system with two identical counter/cross flow plate heat exchangers has been presented. In the numerical model, the bulk mean fluid velocities and temperatures are determined for both the liquid and air sides in each exchanger.

According to the numerical model, the overall effectiveness of the heat recovery system with two identical counter/cross flow heat exchangers is a function of the number of transfer units (*NTU*), the heat capacity rate ratio of the fluids (*Cr*), the aspect ratio of the exchangers (y_0/x_0), and the entrance ratio of the exchangers (x_i/x_0).

The accuracy of the model is verified using correlations from the published literatures for heat exchangers and run-around heat recovery systems using air-liquid cross flow and counter-flow arrangements. Comparisons show that the discrepancy between the predicted effectiveness determined from the numerical model and the effectiveness determined from the correlations is less than ±2.5% for the heat exchangers and run-around systems. This verified model is used to develop a new correlation for the flat-plate counter/cross flow heat exchangers (Eq. (21)).

The new correlation agrees with the numerical model within ±2% for single heat exchangers and run-around systems employing two identical counter/cross flow heat exchangers when the liquid header length to exchanger length ratio is less than 0.25. These performance correlations can be used in engineering designs to predict the performance of counter/cross flow heat exchangers and run-around heat recovery systems under a range of operating conditions and design parameters.

With heat exchangers of equal surface area, the effectiveness of the counter/cross flow heat exchanger is less than that of the counter-flow exchanger, but greater than that of the cross flow exchanger. To achieve a high effectiveness, such as more than 60%, for the

counter/cross RAHE, *NTU* should be larger than 3, C_L/C_A in range of 0.8–1.2, the exchanger aspect ratio should be less than 0.3 and the liquid inlet/outlet header length ratio should be less than 0.25.

References

[1] ASHRAE, 2005 ASHRAE Handbook-Fundamentals, American Society of Heating, Refrigerating and Air Conditioning, Engineers Inc., Atlanta, 2005.

[2] M. Fauchoux, C.J. Simonson, D.A. Torvi, The effect of energy recovery on perceived air quality, energy consumption and economics of an office building, ASHRAE Trans. 113 (2) (2007) 437–449.

[3] A.L. London, W.M. Kays, The liquid-coupled indirect-transfer regenerator for gas-turbine plants, ASME Trans. 73 (1951) 529–542.

[4] B.I. Forsyth, R.W. Besant, The design of a run-around heat recovery system, ASHRAE Trans. 94 (2) (1988) 511–531.

[5] B.I. Forsyth, R.W. Besant, The performance of a run-around heat recovery system using aqueous glycol as a coupling liquid, ASHRAE Trans. 94 (2) (1988) 532–545.

[6] I.J.D. Bennett, R.W. Besant, G.J. Schoenau, Validation of a run-around heat recovery system model, ASHRAE Trans. 100 (1) (1994) 230–237.

[7] I.J.D. Bennett, R.W. Besant, G.J. Schoenau, A.B. Johnson, Procedure for optimizing coils in a runaround heat exchanger system, ASHRAE Trans. 100 (1) (1994) 442–451.

[8] P. Dhital, R.W. Besant, G.J. Schoenau, Integrating run-around heat exchanger systems into the design of large office buildings, ASHRAE Trans. 101 (2) (1995) 979–991.

[9] H. Fan, C.J. Simonson, R.W. Besant, W. Shang, Run-around heat recovery system using cross-flow flat-plate heat exchangers with aqueous ethylene glycol as the coupling fluid, ASHRAE Trans. 111 (1) (2005) 901–910.

[10] H. Fan, C.J. Simonson, R.W. Besant, W. Shang, Performance of a run-around system for HVAC heat and moisture transfer applications using cross-flow plate exchangers coupled with aqueous lithium bromide, HVAC&R Res. 12 (2) (2006) 313–336.

[11] W.M. Kays, A.L. London, Compact Heat Exchangers, third ed., McGraw-Hill, Toronto, 1984.

[12] T. Kuppan, Heat Exchanger Design Handbook, Marcel Dekker, New York, 2000. pp. 27–129.

[13] F.P. Incropera, D.P. Dewitt, Fundamentals of Heat and Mass Transfer, fifth ed., John Wiley & Sons, New York, 2002. pp. 466–509, 642–681.

[14] X. Luo, W. Roetzel, Theoretical investigation on cross-flow heat exchangers with axial dispersion in one fluid, Revue générale de thermique 37 (3) (1998) 223–233.

[15] J.M. Robertson, Hydrodynamics in Theory and Application, Prentice-Hall, Inc./Englewood Cliffs, NJ, 1965. pp. 86–89, 228–238.

[16] Y.Y. Zeng, R.W. Besant, K.S. Rezkallah, The effect of temperature-dependent properties on the performance of run-around heat recovery systems using aqueous-glycol coupling fluids, ASHRAE Trans. 98 (I) (1992) 551–562.